Journal of the Serbian Chemical Society
JSCS-info@shd.org.rs • www.shd.org.rs/JSCS
J. Serb. Chem. Soc. *88* (2) 153–167 (2023)
JSCS–5617
Original scientific paper
Published 22 July 2022

Diagnostics of laser-induced plasma from a thin film of oil on a silica wafer

MILICA VINIĆ[1], MIROSLAV KUZMANOVIC[2#], JELENA SAVOVIC[3#] and MILIVOJE IVKOVIC[1]*

[1]*Institute of Physics, University of Belgrade, Belgrade, Serbia,* [2]*Faculty of Physical Chemistry, University of Belgrade, Belgrade, Serbia and* [3]*Vinča Institute of Nuclear Sciences, University of Belgrade, Belgrade, Serbia*

(Received 28 December 2021, revised 21 March, accepted 23 March 2022)

Abstract: In this study, plasma induced by a nanosecond Nd:YAG laser on thin oil films deposited on a silica wafer was characterized by evaluating the main plasma parameters. Spatially and temporally integrated spectral measurements were performed under experimental conditions optimized for elemental analysis of trace metals in oil. Time-resolved values of the spectral line intensities, electron number density, and plasma temperature were obtained from time-integrated measurements by subtracting averaged spectra recorded at different time delays. The electron number density was estimated using the Stark broadened profile of the hydrogen Balmer alpha line. Ionization temperatures were derived from Mg ionic to atomic line intensity ratios. The obtained apparent values of time-resolved plasma parameters were in the range of 1.1×10^{17} cm^{-3} (1.5 μs) to 1.5×10^{16} cm^{-3} (4 μs) and 9400 K (3 μs) to 7200 K (5 μs), depending on the delay time. Emission spectra of C_2 and CN molecules were used to evaluate the rotational and vibrational temperature.

Keywords: electron number density; plasma temperature; time-integrated; time-resolved.

INTRODUCTION

Laser-induced breakdown spectroscopy (LIBS) is a technique widely used for the multi-elemental analysis of complex samples by detecting spectrally resolved emission of plasma formed after laser ablation of the material. Advantages of the LIBS method include simple, or none sample preparation, fast measurements, capability to detect light elements, non-invasiveness, a possibility for *in-situ* measurements, and relatively high sensitivity.[1–4] While applying LIBS on solid materials is straightforward, analysis of liquid samples can be pretty com-

* Corresponding author. E-mail: ivke@ipb.ac.rs
# Serbian Chemical Society member.
https://doi.org/10.2298/JSC211228028V

plex due to experimental difficulties, such as laser-induced splashing and bubbling. This leads to reduced analytical capability of the LIBS technique, which could be improved by a proper experimental approach and sample preparation.[5–8] The choice of the sampling method is guided by the system complexity, the desired detection limits and precision, and the sample availability.

Laser ablation of a free liquid surface is the most straightforward approach, but the main problem is the production of splashes which require continuous cleaning of nearby optical elements.[6] Also, splashes rapidly consume liquid, so the necessary sample volume for analysis is above typically 1 mL. Liquid splashes can be reduced by analysing slowly flowing liquid[9,10] or almost eliminated by ablating the liquid jet.[11–13] Disadvantages of these approaches are the large, requested sample volumes (>10 mL) and the necessity of washing the circuit before introducing a new sample.

In this work, parameters of plasma formed by ablation of thin oil films deposited on a silica wafer substrate[8] were explored. The preferred oil film thickness was managed by controlling the speed of rotation of samples during the preparation phase. Hydrogen Balmer alpha line (H_α) was used to determine electron number density N_e. Spectral line intensity ratios of the successive ionization stages of the magnesium have been used to determine ionization temperature, T_{ion}. The temperature of heavy particles in the plasma (rotational temperature, T_{rot}, and vibrational temperature, T_{vib}) was estimated by comparing the experimental and simulated emission spectra of C_2 and CN molecules. In addition, time evolutions of the spectral intensities, electron number density, and temperature were deduced from time-integrated measurements by subtracting averaged spectra obtained at different time delays.[14] We must have in mind that all spectral measurements reported in this work were spatially integrated. Therefore, all plasma parameters (N_e, T_{ion}, T_{rot} and T_{vib}) determined in this work, including the calculated time-resolved values, are the apparent values of these parameters. For inhomogeneous spectrochemical sources such as laser-induced plasma, the parameters resulting from spatially integrated measurements represent population averages of the local temperature and electron number density values, *i.e.*, they describe the source but are different from the local values.[15] True plasma parameters, *i.e.*, spatial and temporal distribution of plasma parameters, were difficult to determine due to small plasma volume, large gradients of T and N_e, and the limited reproducibility of emission intensity measurements.

EXPERIMENTAL

Materials and methods

In this experiment, pure reference oil (Base Oil 75, further in the text referred to as Oil-0) and standard oil for spectroscopy measurements (SpexCertiPrep) containing 21 elements (Ag, Al, B, Ba, Ca, Cd, Cr, Cu, Fe, Mg, Mn, Mo, Na, Ni, P, Pb, Si, Sn, Ti, V and Zn) were analysed. The concentration of each element present in oil was of 100 ppm (further in the text

referred to as Oil-100). Oil samples were prepared in the form of thin films by placing a small drop of oil (0.3 μL) on a silica wafer (Graphene Supermarket, W-5P-300) cut into pieces with dimensions of 15 mm×15 mm. The silica wafer was glued on an aluminium disk that matched the spin-coater (Laurell Technologies, KL-SCI-20) and then rotated. When the maximum speed of rotation (150 rps) was used for 30 s, a minimal thickness of oil films (0.74 μm) was obtained. Detailed explanations about selecting optimal conditions for sample preparation can be found elsewhere.[8]

In the following, the substrate on the disk was transferred under the LIBS instrument and scanned.

LIBS system

Fig. 1 illustrates the experimental setup. Nd:YAG laser (Quantel, CFR Ultra) emitting 6.5 ns long pulses at 1064 nm was used to induce plasma. The laser beam with a diameter of 6 mm was guided utilizing two mirrors (M1, M2) and beam expander 2.7X (BE) placed between them. Plano-convex quartz lens (L) with focal length f = 100 mm and a 2" diameter was used to focus laser light perpendicularly to the sample, thus obtaining a spot diameter of 0.72 mm. The LIBS measurements were performed with the maximum incident laser energy of 165 mJ, corresponding to the laser fluence of 40.3 J cm^{-2} or 6.2 GW cm^{-2}.

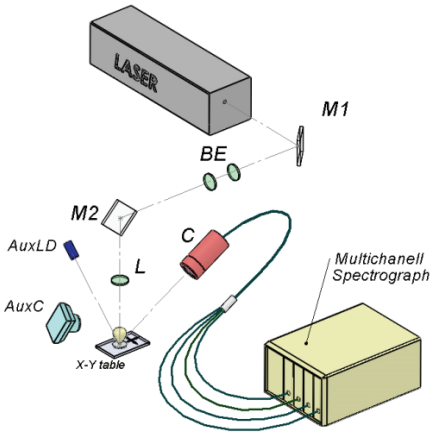

Fig. 1. Experimental setup. M1 and M2 are bending mirrors; BE is beam expander; L is focusing lens; AuxC is video-camera, AuxLD is pointing red diode laser (λ = 635 nm), and C is an optical system for the signal collection.

Plasma emission was then brought to four compact spectrometers (Avantes AvaSpec--ULS2048L), equipped with a grating with a groove density of 2400 or 3600 grooves mm^{-1}. The entrance slits of spectrometers were 10 μm. The spectrometer array covers the spectral range between 200 and 796 nm with the spectral resolution between 0.07 nm in the UV and 0.16 nm in NIR. A digital delay generator (Quantum Composer 9600+) was employed for the external triggering of the laser flash lamp and Q-Switch. DDG was also used for adjusting the acquisition delay from the laser pulse. The acquisition gate width was 1.050 ms. After each laser pulse, the spectra were recorded to monitor and exclude eventual anomalous shots.

RESULTS AND DISCUSSION

Temporal evolution of atomic, ionic and molecular lines

Depending on the characteristics of the laser pulse, the target, and the analyte of interest, it is convenient to optimize the delay time to obtain the best sig-

nal-to-background ratio. For the setup used in this research, it was shown that the optimal signal acquisition delay time in terms of the signal-to-noise ratio of the analytical lines was of 3 μs for the analysis of metal elements in oil.[8]

Fig. 2a shows the evolution of the spectral intensity of several atomic, ionic and molecular species with delay time, obtained by time-integrated measurements. Spectral emission of these species (H I, Mg I, Mg II, C_2 and CN) was used in this research for plasma diagnostics.

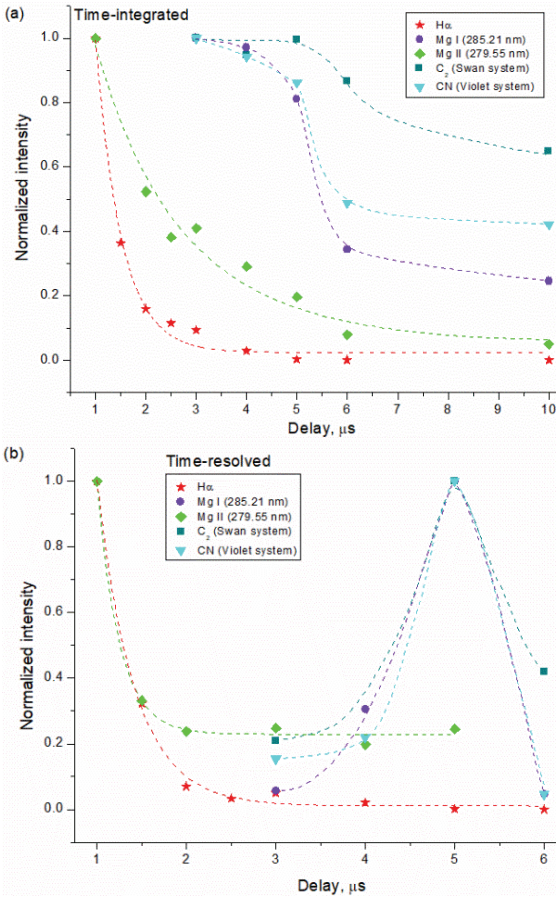

Fig. 2. Spectral line emission intensity of various species in plasma of Oil-100 as a function of time from the laser pulse: a) Time-integrated values and b) calculated time-resolved lines, equivalent to the integration time of 1 μs.

It can be seen in Fig. 2a that the H_α line intensity exponentially decays with the increase of acquisition delay time. The emission intensity of the Mg ionic line also decays exponentially but with the decay rate much slower than H_α. On the other hand, the emission intensity of the neutral Mg spectral line and C_2 and CN molecular emission retain high emission intensity up to around 5 μs and decays exponentially afterward.

The procedure proposed in reference[14] was used to extract time-resolved information from the time-integrated spectra. From a series of the time-integrated emission spectra measured at selected values of delay between the laser pulse and the data acquisition time, the time-resolved emission spectrum was calculated using the following expression:

$$I(t_i)n = \int_{t_i}^{\infty} I(t)\mathrm{d}t - \int_{t_i+n}^{\infty} I(t)\mathrm{d}t \quad (1)$$

where $I(t)$ represents the time-dependent spectral intensity of a given spectral line, t_i is the acquisition delay time, n is a delay interval equivalent to the gate time and $I(t_i)$ is the time-resolved intensity at the delay of t_i. In the present work, the acquisition delay time t_i was varied between 1 and 10 μs, with a step of n = 1 μs.

The calculated time-resolved variation of the spectral intensities as a function of delay time is shown in Fig. 2b. It can be seen that the H_α line emission is concentrated in the initial period of plasma evolution and rapidly exponentially decreases with time. The observed trend was expected because of the high excitation and ionization energies of non-metals. The same trend was observed for the atomic lines of nitrogen and oxygen (not shown in the figure). The Mg II spectral line follows the same trend but decreases more slowly. Due to recombination, which becomes increasingly important by plasma cooling, the intensity of the Mg ionic line decreases over time, while the Mg I line has a maximum at 5 μs and then decreases due to plasma cooling.

Significant emission of C_2 and CN molecular band sequences was registered at 3 μs. At earlier times, the plasma was too hot and did not favor the existence of molecules. Both bands achieve maximum emission at 5 μs and slowly decline afterward, in line with their low excitation energy.

As can be seen from Fig. 2, the calculated time-resolved intensities of the H_α and Mg ionic line (Fig. 2b) show similar profiles as those obtained by time-integrated measurements (Fig. 2a). The only difference is a faster decay of spectral line intensities in the time-resolved evolutions. By contrast, there is a substantial difference in the time-integrated and time-resolved line intensities for Mg I and molecular species. The possible explanation of this difference is as follows. The line profiles in Fig. 2a were obtained from spatially integrated measurements with gate time much longer than the plasma lifetime. Therefore, the measured intensity is composed of contributions from different spatial and time points of the plasma, in which the intensity values are very different. However, the main contribution to the time-integrated spectrum comes from a limited temporal window of the order of the decay time of the emission signal.[14] The emission of ions and high-energy excited atoms decreases faster than the emission signal of neutral atoms and molecules. Moreover, the emission maximum of ions and atoms with high excitation energy is concentrated in the hottest core region, while neut-

ral atoms and molecules populate mainly the plasma periphery. The plasma emission that enters the aperture of the optical fibre may comprise contributions both from the high and low T and N_e regions, whereby these contributions may differ for the short and long delay times. In other words, for short delays, the collected emission may be composed of both high and low T and N_e regions, while at longer delay times, mainly from the low-temperature and low-density regions.

The results presented in Fig. 2b are consistent with the expected behaviour of spectral line intensities due to the expansion and cooling of plasma and recombination processes. These results were further used to obtain the time evolution of the plasma parameters.

Determination of the electron number density

In this work, a standard deconvolution procedure was applied to the observed Voigt-type line profile (w_V) to determine the H_α line Stark width (w_S). The Gaussian fraction is assumed to be a combination of the instrumental and the Doppler broadening, while the Lorentzian component is due to Stark broadening. The Stark width w_S was calculated using the following expression:[16]

$$w_V = 0.5346\ w_L + \sqrt{0.2169\ {w_L}^2 + {w_G}^2}\ ;\ w_G = \sqrt{w_D^2 + w_i^2} \tag{2}$$

where w_V, w_L, w_G, w_D and w_i are the full width at half maximum (FWHM) of the Voigt, Lorentz, Gaussian, Doppler and instrumental profile (experimentally determined), respectively. The contribution of Doppler broadening was found to be negligible for T_g between 10000 and 20000 K.

An approximate formula was then used to calculate N_e / m^{-3}:[17,18]

$$N_e = 10^{23}\left(\frac{w_{SA}}{1.098}\right)^{1.47135} \tag{3}$$

where w_{SA} / nm is the half-width at half area (HWHA) of the H_α spectral line. The H_α line profile is close to Lorentzian, so it was justified to accept $w_{SA} = w_S = w_L$.[17] Finally, it should be pointed out that Eq. (3) differs from the original one,[18] where HWHA was used instead of the claimed.[19]

Fig. 3a shows the H_α line profile recorded at different delay times of the start of signal acquisition.

As expected, considering the high excitation energy of the H_α line, with the delay, both intensity and width of the spectral line profile decrease due to the plasma expansion and cooling. The electron number density calculated from the Stark-broadened H_α line profile (Eq. (3)) shows a rapidly decreasing trend, from 9.5×10^{16} cm^{-3} at gate delay of 1 μs, to 4.7×10^{15} cm^{-3} at a delay of 6 μs. By subtracting the spectra corresponding to different delay times, the temporal evolution of the emission signal and the corresponding electron number density was

roughly reconstructed,[14,20] as shown in Fig. 3b. Differences in time-integrated and time-resolved N_e values originate from different meanings of these values. While in the first case, they represent temporally and spatially averaged values of electron number density, in the second case, they correspond to a particular plasma evolution stage.

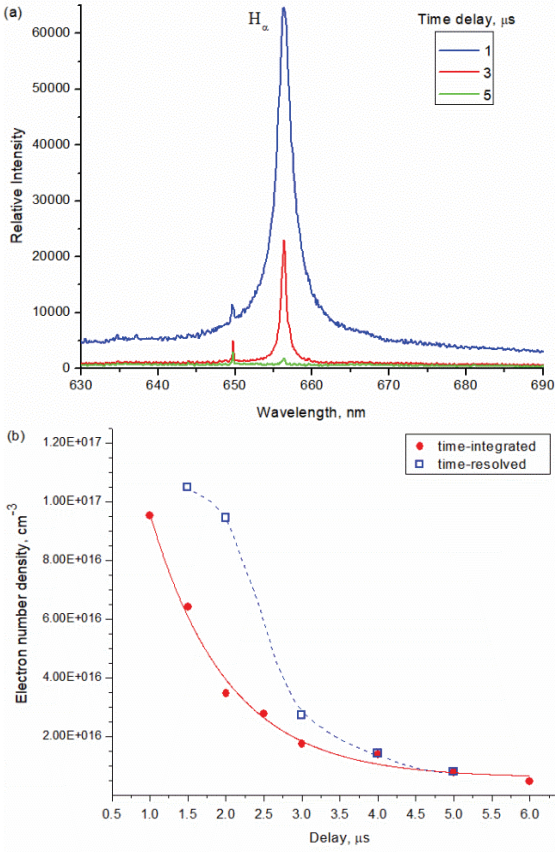

Fig. 3. a) Example of time-integrated H_α line profile at various delays for Oil-100 and b) electron number density at different delays for time-integrated and time-resolved spectra.

Evaluation of plasma temperature

In the oil samples analysed in this paper, the maximum concentration of individual elements was 100 ppm, which was insufficient for the appearance of spectral lines with higher excitation energy that would be suitable for determining T_{exc} using the Boltzmann plot method. Therefore, it was not possible to determine T_{exc} in the plasma of our samples.

Determination of the ionization temperature

The intensity ratio of the ionic and atomic spectral line of the same element is suitable for plasma diagnostics: with a predetermined temperature, the electron

number density can be calculated from it, or vice versa, if the electron number density is predetermined, this approach may be applied for evaluation of the ionization temperature.[21] By substituting the values for physical constants, the expression for the ratio of the integral intensities of the ionic (+) and atomic line (a) reads:

$$\frac{I^+}{I^a} = 4.83\times10^{15}\frac{g^+A^+\lambda^a}{g^aA^a\lambda^+}\frac{\sqrt{T^3}}{N_e}e^{-\frac{11605\left(E^+_{exc}+E_{ion}-E^a_{exc}-\Delta E_{ion}\right)}{T}} \quad (4)$$

where g^+ and g^a are the corresponding statistical weights of ions and atoms, A^+ and A^a are the transition probabilities, N_e the electron number density in cm^{-3}, T is the temperature in K, E^+_{exc} and E^a_{exc} are the excitation energies in eV*, and E_{ion} and ΔE_{ion} are the ionization energy and the reduction of E_{ion} due to Debye shielding, in eV.

Magnesium lines in the spectral region around 280 nm are very suitable for plasma diagnostics.[22,23] The transition probabilities for the Mg I 285.21 nm, Mg II 280.27 nm, and Mg II 279.55 nm lines were determined with accuracy better than 3 %.[24] By substituting the corresponding constants for the Mg I 285.21 nm and Mg II 279.55 nm lines into Eq. (4), the following expression was obtained:

$$\frac{I^+}{I^a} = 3.48\times10^{15}\frac{\sqrt{T^3}}{N_e}e^{-\frac{11605\left(7.734-\Delta E_{ion}\right)}{T}};\ \Delta E_{ion} = 9.96\times10^{-7}N_e^{1/3} \quad (5)$$

The intensity ratio of the corresponding atomic and ionic lines of Mg was measured at different delay times. Part of the LIBS spectrum in the interval 278 to 286 nm is shown in Fig. 4a. Three peaks fitting by the Gaussian function was applied on lines of interest, and peak area was used for further calculations.

The results presented in this work were obtained from the intensity ratio of the Mg II 279.55 nm and Mg I 285.21 nm emission lines. It should be noted that the same results were obtained utilizing the ratio of Mg II 280.27 nm and the Mg I 285.21 lines for plasma characterization.

These two Mg II lines have almost the same E_{exc} and values of transition probability A and differ only by the g values (4 and 2 for Mg II 279.55 nm and Mg II 280.27, respectively). Thus, to utilize data for the measured intensity ratio of Mg II 280.27 nm and Mg I 285.21 nm lines, it is sufficient to divide by 2 the constant ($3.48\cdot10^{15}$) from Eq. (5).

The obtained dependence of T_{ion} on the delay time shows that the temperature decreases from the value of ~8800 K corresponding to a delay of 2 μs to ~6900 K at 6 μs, Fig. 4b. The observed trend was expected considering the plasma expansion and cooling over time. Since they were estimated from time-

* 1 eV = 1.602×10^{-19} J

-integrated measurements, the obtained T_{ion} values represent the averaged values of this plasma parameter and differ from the calculated time-resolved values that characterize a particular plasma evolution stage.

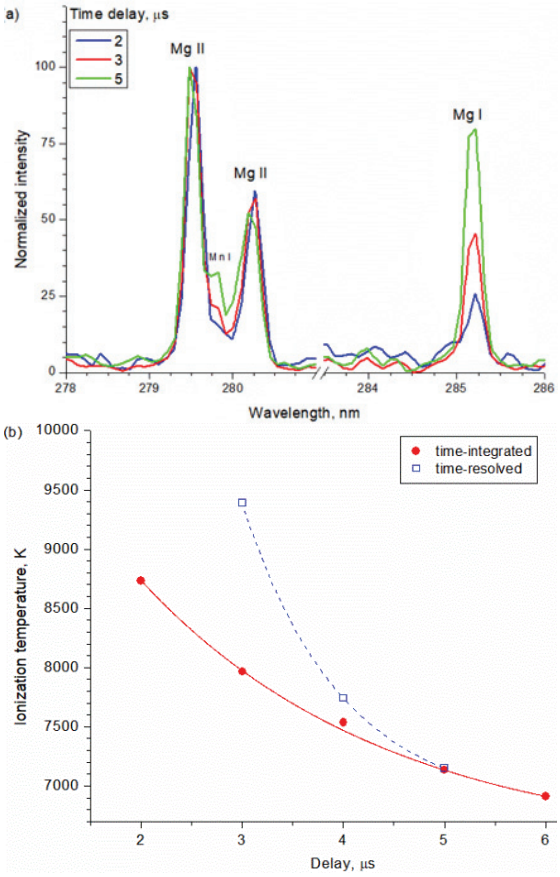

Fig. 4. a) Part of the LIBS spectrum of Oil-100 showing Mg emission lines; b) the ionization temperature as a function of the delay time for Oil-100.

Determination of rotational and vibrational temperatures

Apart from the atomic emission, LIBS spectra of the oil film deposited on a silicon substrate were dominated by high-intensity emission bands corresponding to CN and C_2 molecules. Due to the relatively high dissociation energies (7.72 eV for CN, and 6.27 eV for C_2),[25] low excitation potentials, and favourable transition probabilities, the CN violet system and C_2 Swan system bands can be readily observed in the LIBS spectra of carbon-containing materials. As it is seen in Fig. 5, intense CN molecular bands corresponding to $\Delta\nu$ 0, –1 and +1 sequence were registered. The figure also shows C_2 molecular bands corresponding to $\Delta\nu = 0$ and $\Delta\nu = +1$ sequence with (0-0) band head at 516.52 nm, and $\Delta\nu =$ $= +1$ with (1-0) band head at 473.71 nm, which were of somewhat lower int-

ensity. The $\Delta v = -1$ sequence with (0-1) band head at 563.55 nm, located in the spectral region 546–570 nm, could not be registered using the present setup.

The resolution of the used spectrometers was not high enough to provide a well-resolved rotational structure of the registered CN molecular bands. Therefore, these bands were unsuitable for the determination of the rotational temperature. Differently, vibrational band heads of the $\Delta v = 0$ and $\Delta v = -1$ sequences were sufficiently resolved, which allowed their use for the estimation of the vibrational temperature.

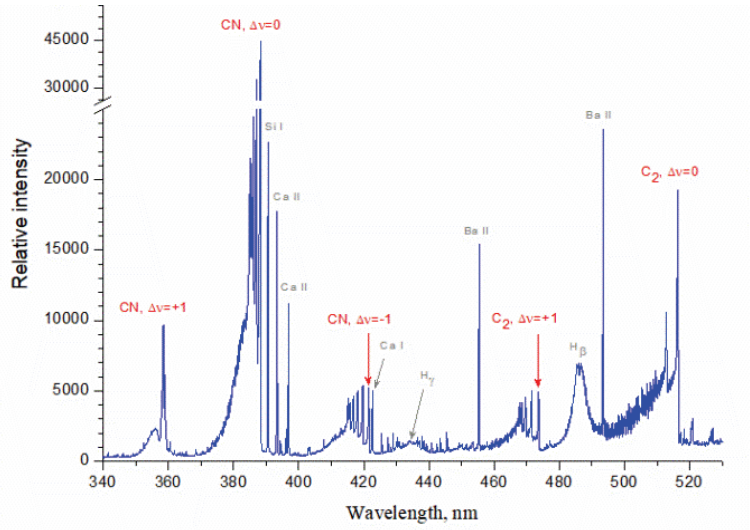

Fig. 5. Part of the time-integrated LIBS spectra of Oil-100 sample showing characteristic emission bands of C_2 and CN molecules.

Fig. 6a compares the experimental spectrum of the sample Oil-5 and synthetic spectra of the $\Delta v = -1$ sequence calculated for several different temperatures. The synthetic spectra were obtained using the program LIFBASE 2.1.1,[26] with a pure Gaussian line profile of 0.173 nm, as determined by deconvolution of the adjacent analyte (metal) spectral lines and assuming the rotational and vibrational temperature were equal. The instrumental profile estimated using the oil sample with a doped concentration of the analyte elements of 5 ppm was the same as that determined using the Argon spectral calibration lamp. All spectra were normalized to the intensity of the (0-1) band head. It is evident that the widths of the experimental and synthetic band heads were the same, implying an insignificant influence of self-absorption. The vibrational temperature was estimated at 5800 K with an error lower than 500 K. Approximately the same value for the rotational temperature could be estimated from the spectrum between the

(1-2) and (0-1) band heads (whose intensity entirely depends on the rotational temperature), although certainly with much lower accuracy.

In the $\Delta v = +1$ sequence of C_2 Swan system, five well-separated band heads were registered, suitable for determining the vibrational temperature because their relative intensity ratios are markedly dependent on temperature. Fig. 6b compares the normalized synthetic spectra for several temperatures (assuming that the vibrational and rotational temperatures are equal), with a pure Gaussian profile of 0.14 nm (determined experimentally) with an experimental spectrum of the Oil-0 sample. The synthetic spectra were obtained using the program PGOPHER 10.1.182.[27] As it can be seen in Fig. 6b, self-absorption can be neglected because the widths of the corresponding experimental and theoretical profiles coincide. The vibrational temperature was estimated at 4800 K, with an error lower than 300 K. An increase of the acquisition delay time, from 3 to 10 μs, showed a small but measurable trend of decreasing vibrational temperature. For a given delay time interval, the vibrational temperature decreased by approximately 700 K.

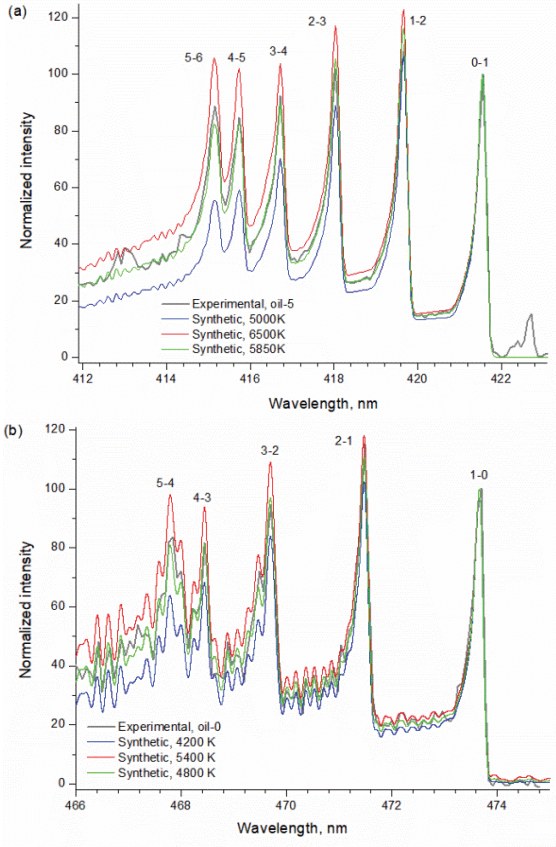

Fig. 6. Comparison of the experimental and synthetic spectra of the: a) CN violet system $\Delta v = -1$ sequence for Oil-5 and b) C_2 Swan system $\Delta v = +1$ sequence for Oil-0.

The difference in the temperatures estimated from the CN bands (5850 K) and C_2 bands (4800 K) indicates a different plasma zone from which CN and C_2 bands are predominantly emitted, which is partly related to a slightly higher excitation and dissociation energy of CN molecule (E_{exc} = 3.19 eV, E_{dis} = 7.8 eV) relative to the C_2 molecule (E_{exc} = 2.39 eV, E_{dis} = 6.2 eV).[28] Also, the difference may be due to the different time evolution of the emission bands, where the C_2 emission has a maximum at 5 μs and a slower decay time than CN (Fig. 2). Thus, the calculated temperatures for C_2 from the integrated spectra are characteristic for later stages of the plasma evolution. The difference may also be a consequence of different formation mechanisms for these two molecular species. Due to much smaller energy differences between adjacent vibrational, and especially rotational levels of molecules compared to differences in electronic states of free atoms, it is assumed that rotational and vibrational temperatures correspond to the temperature of heavy particles in the plasma (*i.e.*, the gas temperature).[29] The $\Delta v = 0$ sequences of both systems were not used for temperature estimation because they show significant self-absorption.

The difference between the temperatures determined from the molecular bands and using the emission of atomic and ionic lines is a consequence of the fact that plasma emission was registered spatially and temporally integrated. At the same time, molecules, atoms, and ions have their maximum emission intensity in plasma zones characterized by different temperatures.

The difference between the temperatures determined from the molecular bands and using the emission of atomic and ionic lines is a consequence of the fact that plasma emission was registered spatially and temporally integrated. At the same time, molecules, atoms, and ions have their maximum emission intensity in plasma zones characterized by different temperatures.

CONCLUSIONS

Time-integrated and time-resolved spectral line intensities imply that the emission of nonmetals and metal ions (H I and Mg II) are more intense in the earlier stages of plasma evolution. In contrast, the emission of atomic and molecular band lines occurs later, reaching maximum intensity at around 5 μs. Apparent values of electron number density (derived from time-integrated measurements of the H_α line profile) rapidly decrease from 9.5×10^{16} cm^{-3} at gate delay of 1 μs to 4.7×10^{15} cm^{-3} at a delay of 6 μs. The estimated time-resolved values for N_e show a similar declining trend. Ionization temperature (derived from Mg II/Mg I spectral line intensity ratio) also shows a declining trend with time. For time-integrated measurements, T_{ion} decreases from 8800 K at gate delay of 2 μs to 6900 K at a delay of 6 μs. Similar to the N_e values, the time-resolved values of T_{ion} have higher values and decrease faster than time-integrated values. The observed difference is understandable since time-integrated measurements represent

temporally and spatially averaged plasma parameters, while time-resolved values correspond to a particular plasma evolution stage.

Evaluation of the vibrational-rotational temperature from the molecular bands spectra gave different values for CN (5800 K) and C_2 molecules (4800 K), probably due to different formation mechanisms of these two molecular species and a difference in their dissociation and excitation energies. Increasing the detection delay time causes a slight decrease of the estimated temperature, about 700 K, for a delay time change from 3 to 10 μs.

Acknowledgments. The research was funded by the Ministry of Education, Science and Technological Development of the Republic of Serbia, Contract numbers: 451-03-9/2021-14/200024, 451-03-9/2021-14/200146, and 451-03-9/2021-14/200017. Milica Vinic acknowledges ENEA (Italy) for supporting her work on the collection of experimental data presented in this work. The authors acknowledge Dr. Violeta Lazić from ENEA (Italy) for providing the experimental data used in this work and for helpful scientific discussions.

ИЗВОД

ДИЈАГНОСТИКА ПЛАЗМЕ ИНДУКОВАНЕ ДЕЈСТВОМ ЛАСЕРСКОГ ЗРАЧЕЊА НА ТАНКИ ФИЛМ УЉА НА СУПСТРАТУ ОД СИЛИЦИЈУМА

МИЛИЦА ВИНИЋ[1], МИРОСЛАВ КУЗМАНОВИЋ[2], ЈЕЛЕНА САВОВИЋ[3] и МИЛИВОЈЕ ИВКОВИЋ[1]

[1]Институт за физику, Универзитет у Београду, Београд, [2]Факултет за физичку хемију, Универзитет у Београду, Београд и [3]Институт за нуклеарне науке "Винча", Универзитет у Београду, Београд

Тема овог рада је дијагностика плазме која се формира интеракцијом наносекундног Nd:YAG ласера са танким филмом уља нанешеним на супстрат од силицијума. Експериментални услови за спектрална мерења оптимизовани су у сврху елементне анализе метала присутних у траговима. Снимљени спектри су интегрални по простору и времену, али је временски разложене спектре могуће конструисати одузимањем усредњених спектара снимљених са различитим временима кашњења. Густина електрона процењена је из ширине Штарковог профила водоникове Балмер алфа линије. Температура јонизације рачуната је из односа интензитета јонске и атомске линије магнезијума. Процењена привидна вредност густине електрона креће се у опсегу од $1{,}07\times10^{17}$ cm^{-3} (за 1,5 μs) до $1{,}5\times10^{16}$ cm^{-3} (за 4 μs). Процењена привидна вредност температуре јонизације креће се у опсегу од 9400 K (за 3 μs) до 7200 K (за 5 μs). Из емисионих спектара C2 и CN молекула процењена је ротациона и вибрациона температура.

(Примљено 22. децембра 2021, ревидирано 21. марта, прихваћено 23. марта 2022)

REFERENCES

1. D. A. Cremers, R. C. Chinni, *Appl. Spectrosc. Rev.* **44** (2009) 457 (https://dx.doi.org/10.1080/05704920903058755)
2. R. Noll, *Laser-Induced Breakdown Spectroscopy*, Springer, Heidelberg, 2012 (https://dx.doi.org/10.1007/978-3-642-20668-9)
3. D. W. Hahn, N. Omenetto, *Appl. Spectrosc.* **64** (2010) 335A (https://dx.doi.org/10.1366/000370210793561691)

4. D. W. Hahn, N. Omenetto, *Appl. Spectrosc.* **66** (2012) 347 (https://dx.doi.org/10.1366/11-06574)
5. V. Lazic, in *Laser-Induced Breakdown Spectroscopy*, S. Musazzi, U. Perini (Eds.), Springer-Verlag, Berlin, 2014, p. 195 (https://doi.org/10.1007/978-3-642-45085-3_8)
6. V. Lazic, R. Fantoni, A. Palucci, M. Ciaffi, *Appl. Spectrosc.* **71** (2017) 670 (https://dx.doi.org/10.1177/0003702816685096)
7. N. Aras, Ş. Yalçın, *Talanta* **149** (2016) 53 (https://dx.doi.org/10.1016/j.talanta.2015.11.031)
8. M. Vinić, E. Aruffo, F. Andreoli, M. Ivković, V. Lazic, *Spectrochim. Acta, B* **164** (2020) 105765 (https://dx.doi.org/10.1016/j.sab.2020.105765)
9. K. Rifai, S. Laville, F. Vidal, M. Sabsabi, M. Chaker, *J. Anal. At. Spectrom.* **27** (2012) 276 (https://dx.doi.org/10.1039/c1ja10178a)
10. L. St-Onge, E. Kwong, M. Sabsabi, E.B. Vadas, *J. Pharm. Biomed. Anal.* **36** (2004) 277 (https://dx.doi.org/10.1016/j.jpba.2004.06.004)
11. P. Yaroshchyk, R. J. S. Morrison, D. Body, B. L. Chadwick, *Spectrochim. Acta, B* **60** (2005) 986 (https://dx.doi.org/10.1016/j.sab.2005.03.011)
12. N-H. Cheung, E. S. Yeung, *Anal. Chem.* **66** (1994) 929 (https://dx.doi.org/10.1021/ac00079a003)
13. N. K. Rai, A. K. Rai, *J. Hazard. Mater.* **150** (2008) 835 (https://dx.doi.org/10.1016/j.jhazmat.2007.10.044)
14. E. Grifoni, S. Legnaioli, M. Lezzerini, G. Lorenzetti, S. Pagnotta, V. Palleschi, *J. Spectrosc.* **2014** (2014) 1 (https://dx.doi.org/10.1155/2014/849310)
15. C. Aragón, J. A. Aguilera, *Spectrochim. Acta, B* **63** (2008) 893 (https://dx.doi.org/10.1016/j.sab.2008.05.010)
16. J. J. Olivero, R. L. Longbothum, *J. Quant. Spectrosc. Radiat. Transf.* **17** (1977) 233 (https://dx.doi.org/10.1016/0022-4073(77)90161-3)
17. N. Konjević, M. Ivković, N. Sakan, *Spectrochim. Acta, B* **76** (2012) 16 (https://dx.doi.org/10.1016/j.sab.2012.06.026)
18. M. A. Gigosos, M. A. González, V. Cardeñoso, *Spectrochim. Acta, B* **58** (2003) 1489 (https://dx.doi.org/10.1016/S0584-8547(03)00097-1)
19. M. A. Gonzalez, *private communication* (2012)
20. R. Ahmed, N. Ahmed, J. Iqbal, M. A. Baig, *Phys. Plasmas* **23** (2016) 083101 (https://dx.doi.org/10.1063/1.4959866)
21. P. W. J .M. Boumans, *Theory of Spectrochemical Excitation*, Hilger &Watts LTD, London, 1966
22. J. M. Mermet, *Anal. Chim. Acta* **250** (1991) 85 (https://dx.doi.org/10.1016/0003-2670(91)85064-Y)
23. E. Tognoni, M. Hidalgo, A. Canals, G. Cristoforetti, S. Legnaioli, A. Salvetti, V. Palleschi, *Spectrochim. Acta, B* **62** (2007) 435 (https://dx.doi.org/10.1016/j.sab.2007.05.006)
24. W. Ansbacher, Y. Li, E. H. Pinnington, *Phys. Lett., A* **139** (1989) 165 (https://dx.doi.org/10.1016/0375-9601(89)90353-8)
25. A. D. Pradhan, H. Partridge, C. W. Bauschlicher, *J. Chem. Phys.* **101** (1994) 3857 (https://dx.doi.org/10.1063/1.467503)
26. J. Luque, D. R. Crosley, *SRI Int. MP* **99** (1999) https://www.sri.com/engage/products-solutions/lifbase

27. C . M .Western, *J. Quant. Spectrosc. Radiat. Transf.* **186** (2017) 221 (https://dx.doi.org/10.1016/j.jqsrt.2016.04.010)
28. A. De Giacomo, J. Hermann, *J. Phys., D* **50** (2017) 183002 (https://dx.doi.org/10.1088/1361-6463/aa6585)
29. M. Venugopalan, *Reactions under plasma conditions*, John Wiley and Sons, Inc, New York, 1971.